Structural impact on the methano bridge in norbornadiene, norbornene and norbornane

ARTICLE *in* JOURNAL OF PHYSICS AND CHEMISTRY OF SOLIDS · DECEMBER 2004

Impact Factor: 1.85 · DOI: 10.1016/j.jpcs.2004.08.018

3 AUTHORS, INCLUDING:

Feng WANG
Swinburne University of Technology
208 PUBLICATIONS **1,596** CITATIONS
SEE PROFILE

David Alan Winkler
The Commonwealth Scientific and Industri…
164 PUBLICATIONS **2,522** CITATIONS
SEE PROFILE

Available online at www.sciencedirect.com
SCIENCE DIRECT®
Journal of Physics and Chemistry of Solids 65 (2004) 2041–2054
JOURNAL OF PHYSICS AND CHEMISTRY OF SOLIDS
www.elsevier.com/locate/jpcs

Structural impact on the methano bridge in norbornadiene, norbornene and norbornane

F. Wang[a], M.J. Brunger[b,*], D.A. Winkler[c]

[a]Centre for Molecular Simulation, Swinburne University of Technology, Hawthorn, Melbourne, Vic. 3122, Australia
[b]Department of Physics, School of Chemistry, Physics and Earth Sciences, Flinders University, GPO Box 2100, Adelaide, SA 5001, Australia
[c]Division of Molecular Sciences, CSIRO, Private Bag 10, Clayton South MDC, Vic. 3169, Australia

Abstract

An electronic structural study of the ground electronic states for the chemically similar bicyclic norbornadiene (NBD, C_7H_8, X^1A_1), norbornene (NBN, C_7H_{10}, X^1A') and norbornane (NBA, C_7H_{12}, X^1A_1) molecules is provided quantum mechanically. Initially, the unique orbital imaging capability of electron momentum spectroscopy is used to validate which of the quantum mechanical models available to us for these calculations best represents these species. Thereafter, individual molecular point group symmetry is incorporated in the calculations with energy minimization in the search for equilibrium geometries of the species using MP2/TZVP and B3LYP/TZVP models. The optimized geometries compare favourably with available crystallographic results and also build confidence in cases where the crystallographic results are ambiguous. The present study aims to reveal the particular subtle structural deviation of the species, which results in significant molecular property differences among these organic compounds. This work intends to probe bonding information of the species and the impact, on the seven member carbon skeleton, as the C=C double bonds of NBD are progressively saturated by hydrogen atoms to give NBN and NBA. Significant changes observed through the present work include: (i) the seven member carbon skeleton tends to relax the strain whenever possible and (ii) the ethano ring experiences greater structural changes than the methano bridge. The methano bridge ($C_{(1)}$–$C_{(7)}$–$C_{(4)}$) of the less symmetric NBN molecule (C_s) tilts to the single C–C bond side of the ethano ring of the molecule (rather than the C=C side), producing a dihedral angle of 8.7° between plane H–$C_{(1)}$–$C_{(4)}$ (the *yz*-plane) and plane $C_{(1)}$–$C_{(7)}$–$C_{(4)}$. Our work suggests that it is this unique dihedral angle in NBN which causes the molecules exo-reactivity and is also responsible for the extra activity of its C=C bond.

1. Introduction

The chemically similar, highly strained, bicyclic hydrocarbons norbornadiene (C_7H_8, NBD), norbornene (C_7H_{10}, NBN) and norbornane (C_7H_{12}, NBA) comprise one of the key groups of compounds in structural and synthetic chemistry. The rigid bicycle carbon skeleton of the three species has often been employed to fix geometric variables in structure/reactivity studies, as well as in the investigation of the relationship between structural and spectroscopic properties [1]. The six-membered (ethano) ring is held in a boat conformation and thus serves as a model for the transition state for chair–chair inter-conversion in synthetic chemically important six-membered rings [1]. Moreover, the bridging $C_{(7)}$ atom subtends a less than optimum angle (109.47°) for a saturated linkage and hence is expected to be a major contributor to strain effects. Owing to their globular nature and the absence of strong, directional intermolecular forces, the three species are orientationally disordered, and exhibit plastic phases at ambient temperature and pressure [2]. However, other molecular properties such as chemical reactivity differ significantly between these species. A detailed knowledge of their electronic structures could reveal how molecular bonding information responds to their substantial strains and how their significantly different properties could reflect their subtle structural differences.

It is well known that the molecular properties of species depend critically on their detailed electronic structures. The three species studied here are associated in a close relationship: point group C_{2v} for both unsaturated NBD and saturated NBA and point group C_s for NBN. Norbornane (C_{2v}) is a key compound in structural chemistry and it demonstrates challenges to crystallographic structural

* Corresponding author. Tel.: +61 8 8201 2958; fax: +61 8 8201 2905.
E-mail address: michael.brunger@flinders.edu.au (M.J. Brunger).

0022-3697/$ - see front matter © 2004 Elsevier Ltd. All rights reserved.
doi:10.1016/j.jpcs.2004.08.018

determinations. Its derivatives have held a prominent position in the investigation of phenomena associated with non-classical ions [3], such properties of bicyclic compounds wherein they differ from the corresponding acyclic alkane are rationalized in terms of several types of 'strain' imposed by their geometries. Bicyclic molecules are also of interest because, compared to acyclic species, the relatively rigid structures of the carbon skeleton lead to unambiguous orientations and magnitudes of separation of substitutions. The absence of complications from considering averages over several widely different conformations has additionally made this group of molecular species attractive for testing numerous models [4].

A C=C double bond is usually planar: the two carbon atoms with sp^2 hybridization, and the four atoms attached to them lie in a common plane. However, if the double bonds are incorporated into strained bicyclic systems, such as NBN and NBD, considerable deviations from planarity of double bonds can occur. Hence if the bond angles deviate from those idealized bond angles of 109.47 and 120.0° for hybridized carbons, the molecules become strained. The seven-member unsaturated species (NBN and NBD) do not have a plane of symmetry passing through the sp^2 carbons so that their double carbon bonds are associated with non-planarity and strain. The experimental exo-reactivity related to the double bond of the NBN molecule has puzzled chemists for many years [5]. Norbornene is considered as one of the prototype strained olefins, due to its extreme chemical reactivity, undergoing elimination, dimerisation, addition and isomerisation [6], as well as exo-selectivity [7]. Norbornadiene (NBD), on the other hand, is an unconjugated, strained and non-planar diene. It is a prototype for through space and through bond interaction studies, with our recent electron momentum spectroscopy (EMS) study confirming the through space interaction dominance in NBD [8,9].

There are many possible quantum mechanical (QM) models that we could employ in the electronic structure calculations of this paper. It would therefore be nice to have an a priori indication of which of these QM models might provide a reliable representation of the molecules in question. The unique orbital imaging capability of EMS [8,9] provides us with a mechanism for achieving precisely this. In this technique EMS measures orbital momentum densities (MDs) for the molecular orbitals of the species in question, and these are then compared in detail to those correspondingly calculated using the available basis states (from e.g. GAUSSIAN, GAMESS or DGAUSS). On the basis of this rather detailed comparison optimum models for the species of interest can thus be determined and then used in our detailed electronic structural calculations.

2. Experimental and theoretical EMS details

The 18 molecular orbitals (MOs) of the complete valence region of NBD, 19 MOs of NBN and 20 MOs of NBA were, respectively, investigated in a series of experimental runs using the Flinders symmetric non-coplanar EMS spectrometer. Details of this coincidence spectrometer and the method of taking the data can be found in Brunger and Adcock [10] and Weigold and McCarthy [11] and so we do not repeat them again here.

The high purity (>99.5%) sample (NBD, NBN or NBA) is admitted into the target chamber through a capillary tube, the flow rate being controlled by a variable leak valve. Note that the molecular driving pressure in each case was too low to cause any significant clustering by supersonic expansion. The collision region is differentially pumped by a 700 l s^{-1} diffusion pump. Apertures and slits are cut in the collision chamber for the incident beam and scattered and ejected electrons. The differentially pumped collision region makes it possible to increase the target gas density by a factor of about 3 while keeping the background pressure in the spectrometer below 10^{-5} Torr. This was important as it enabled us to maintain workable coincidence count rates, even with the relatively smaller electron beam current output from the (e,2e) monochromator (typically ~25 μA) compared to that of a normal electron gun (~100 μA). The coincident energy resolution in the present series of measurements was typically in the range 0.5−0.6 eV full-width-at-half-maximum (FWHM), as determined from measurements of the binding-energy (ε_f) spectrum of helium. However, due to the natural-line widths of the various transitions as estimated from the relevant photoelectron spectroscopy (PES) spectra [12–14], the fitted resolutions of the spectral peaks for NBD, NBN or NBA varied from 0.71 to 2.305 eV (FWHM). It is precisely this limitation which forces us to, occasionally, combine our measured MDs in each of the molecules studied, e.g. for NBD we combined the respective $2a_2$ and $4b_1$ orbital MDs, $3b_1$ and $5a_1$ orbital MDs, $2b_1$ and $4a_1$ orbital MDs, $1a_2$ and $3a_1$ orbital MDs and $2a_1$ and $1b_1$ orbital MDs. While such a process necessarily loses a degree of the available physical information [46], to do otherwise would have raised serious doubts as to the uniqueness of the MDs derived in our spectral deconvolution fit to the measured binding-energy spectra (see below). The angular resolution, which determines the momentum resolution [10,11], was typically 1.2° (FWHM), as determined from the electron optics and apertures and from a consideration of the argon 3p angular correlation.

In the current series of measurements for NBD, NBN and NBA, non-coplanar symmetric kinematics were employed, that is, the outgoing electron energies E_A and E_B were equal, and the scattered (A) and ejected (B) electrons made equal polar angles $\theta = 45°$ with respect to the direction of the incident electrons. The total energy (E), $E = E_A + E_B = E_0 - \varepsilon_f$, was 1500 eV for each molecule. The binding-energy range of interest (ε_f = 6–33 eV for NBD, ε_f = 6–30 eV for NBN and ε_f = 7–29 eV for NBA) is stepped through sequentially and the number of true coincidence (e,2e) counts was recorded at each of a chosen set of angles ϕ using

a binning mode [11]. The range of ϕ used in the present studies was $\phi = 0$–$27.5°$ for NBD, 0–30° for NBN and 0–30° for NBA. Scanning through a range of ϕ is equivalent to sampling different target electron momenta p as

$$p = \left[(2p_A \cos\theta - p_0)^2 + 4p_A^2 \sin^2\theta \sin^2\left(\frac{\phi}{2}\right)\right]^{1/2} \quad (1)$$

where p_0 is the incident electron momentum. For $\varepsilon_f = 0$ eV, $\phi = 0°$ corresponds to $p = 0$ a.u., and for the present binding energies, angular resolution and kinematics, $\phi = 0°$ corresponds to $p \approx 0.03$ a.u. Similarly for $\phi = 10°$, $p \approx 0.92$ a.u. (Note 1 a.u. $\equiv 1a_0^{-1}$, where a_0 = Bohr radius).

The measured binding energy spectra, at each $\phi(p)$ and for each respective molecule, are analysed using a least-squares-fit deconvolution technique from Bevington and Robinson [15]. In all cases the number of free parameters allowed to vary in the fit was minimised. To this end the widths of the respective Gaussians were fixed at a value determined by the convolution of the PES natural widths and the intrinsic energy resolution, while the Gaussian positions (in ε_f) were fixed by the accurate PES values [12–14] for the MOs of each molecule in question. Under these circumstances only the respective peak heights (relative (e,2e) cross-sections ≡ orbital momentum densities) were allowed to vary in the spectral fit. For each molecule excellent fits ($\chi^2 \approx 1$) to the measured binding-energy spectra were generally obtained. This analysis allowed us to derive the required orbital momentum densities for all the respective valence orbitals of NBD, NBN and NBA. Although the measured MDs are not absolute, relative magnitudes for the different transitions of a given molecule are obtained [10]. In the current EMS investigations of the valence states of NBD, NBN and NBA, in each case the experimental MDs are placed on an absolute scale by summing the experimental flux for each measured ϕ for the outer valence orbitals, and then normalising this to the corresponding sum from the results from an appropriate calculation.

Theoretical orbital momentum densities were calculated within the plane wave impulse approximation (PWIA). Using the Born-Oppenheimer approximation for the target and ion wave functions, the EMS orbital momentum density (cross-section) σ, for randomly oriented molecules and unresolved rotational and vibrational states, is given by

$$\sigma = K \int d\Omega |\langle \boldsymbol{p} \Psi_f^{N-1} | \Psi_i^N \rangle|^2 \quad (2)$$

where K is a kinematical factor which is essentially constant in the present experimental arrangement, Ψ_f^{N-1} and Ψ_i^N are the electronic many-body wave functions for the final [$(N-1)$ electron] ion and target [N electron] ground states and $\boldsymbol{p}$ is the momentum of the target (NBD or NBN or NBA) electron at the instant of ionisation. The $\int d\Omega$ denotes an integral over all angles (spherical averaging) due to averaging over all initial rotational states. The average over the initial vibrational state is well approximated by evaluating orbitals at the equilibrium geometry of the molecule. Final rotational and vibrational states are eliminated by closure [11].

The momentum space target-ion overlap $\langle \boldsymbol{p} \Psi_f^{N-1} | \Psi_i^N \rangle$ can be evaluated using configuration interaction descriptions of the many-body wave functions [11], but usually the weak-coupling approximation [11] is made. Here, the target-ion overlap is replaced by the relevant orbital of, typically, the Hartree–Fock (HF) or Kohn–Sham (KS) [16] ground state Φ_0, multiplied by a spectroscopic amplitude. With these approximations Eq. (2) reduces to:

$$\sigma = K S_j^{(f)} \int d\Omega |\Psi_j(\vec{p})|^2 \quad (3)$$

where $\Psi_j(\vec{p})$ is the momentum space orbital for the molecule in question. Eq. (3) explicitly shows the relationship between the orbital momentum density and the orbital wave function and is the basis for the orbital imaging capability of EMS. Note that in (3) the relaxation of the final state has been neglected. The spectroscopic factor $S_j^{(f)}$ is the square of the spectroscopic amplitude for orbital j and ion state f. It satisfied the sum rule:

$$\sum_j S_j^{(f)} = 1 \quad (4)$$

Hence $S_j^{(f)}$ may be considered as the probability of finding the one hole configuration in the many-body wave function of the ion.

There were many possible HF- or DFT-type models that we could employ in our later electronic structural calculations. However, we have previously found [17] that in calculating theoretical orbital momentum densities for larger molecules, DFT-BP/TZVP model is superior (typically) than other models. As a consequence, we restrict our comparison between the theoretical and experimental MDs (in Section 3) to theory results from DFT-BP/TZVP. Note that TZVP is a DGAUSS basis set [47] and DGAUSS is itself part of UniChem, a suite of computational quantum-chemistry programs from ACCELRYS. Employing the UniChem user interface, we built model NBD, NBN and NBA molecules and then employed DGAUSS with various exchange-correlation functionals and basis sets to minimise the total energy of the respective species in their ground electronic states. Information of the molecular structure and molecular orbital wave functions obtained from these DFT calculations were (for each molecule in turn) next treated as input to the Flinders-developed program AMOLD [18], which computes the momentum space spherically averaged molecular-structure factor and the theoretical orbital momentum density (see Eq. (3)).

3. Comparison between experimental and theoretical momentum distributions

The comparisons of calculated orbital momentum densities with experiment may be viewed as an

exceptionally detailed test of the quality of the basis set. The results from this process for some illustrative examples in NBD, NBN and NBA are now presented.

Our EMS results for NBD have been discussed in detail previously [8,9]. Here, we simply reproduce and discuss our experimental and theoretical orbital momentum densities for the $3b_2$ orbital of norbornadiene. In Fig. 1 we see that the shape of the present $3b_2$ MD is interesting, with three local maxima observed at $p \approx 0.04$ a.u., $p \approx 0.3$ a.u. and $p \approx 1.1$ a.u. This result is in good qualitative agreement with each of our PWIA-BLYP/TZVP, -BP/TZVP -BP/DZVP2 and -BP/DZVP calculations. Indeed the shapes of all the computations and that of the experimental MD are in good accord over the entire range of target electron momentum (p). However, when the magnitude of the MDs is considered it is apparent that at $p \approx 0.04$ a.u. all the computations somewhat overestimate the magnitude of the experimental cross-section. As the small momentum region corresponds to the large r (coordinate space) region of the wave function, this indicates that more diffuse functions may be required in the basis sets. Notwithstanding, this Fig. 1 strongly suggests, especially for $p < 0.45$ a.u., that the PWIA calculation with BP/TZVP or BLYP/TZVP exchange-correlation functional/basis does best in reproducing the experimental orbital momentum density. This is a trend we find throughout all the orbitals of this species [8,9]. Finally, we note the good agreement between the measured $3b_2$ cross-sections (MDs) that we obtained in our two independent experiments.

For norbornene a new EMS result for the experimental and theoretical orbital momentum densities of its $6a'' + 11a' + 10a' + 9a' + 5a''$ orbitals is given in Fig. 2. In this case energy resolution limitations and Franck–Condon overlap has meant that a significant number of orbitals have had to be summed. While we agree this necessarily must result in a loss of some physical information [46], important observations can still be made from Fig. 2. In particular we see that the PWIA calculation with LSD/DZVP model significantly overestimates the magnitude of measured cross-sections over all $p \leq 2$ a.u. While LSD/TZVP does a much better job in reproducing the experimental MD it too, for $0.1 < p$ (a.u.) < 0.75, somewhat overestimates the magnitude of the experimental MD. Hence Fig. 2 is interesting in that it not only indicates the superiority of the TZVP basis over the DZVP basis, but it also indicates that generalised gradient approximation (GGA) exchange-correlation functionals should be preferred to the local-spin-density (LSD) approximation exchange-correlation functional. The trends we observe in Fig. 2 are also symptomatic for most of the other orbitals of norbornene.

In Fig. 3 we plot our 1500 eV symmetric non-coplanar experimental and theoretical orbital momentum densities

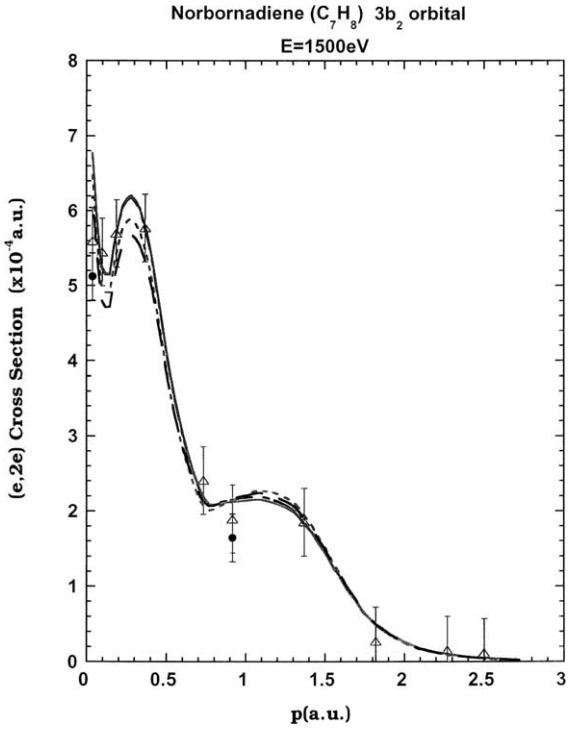

Fig. 1. The 1500 eV symmetric non-coplanar MD for the $3b_2$ orbital of norbornadiene ($\varepsilon_f = 14.3$ eV). The present data for Run A (●) and Run B (△) are compared against the results of our PWIA-DFT calculations: (- -) BLYP/TZVP, (—) BP/TZVP, (- - -) BP/DZVP2 and (– –) BP/DZVP. Reproduced with permission of the American Chemical Society. Note that in this case the BLYP/TZVP and BP/TZVP MD results are very similar.

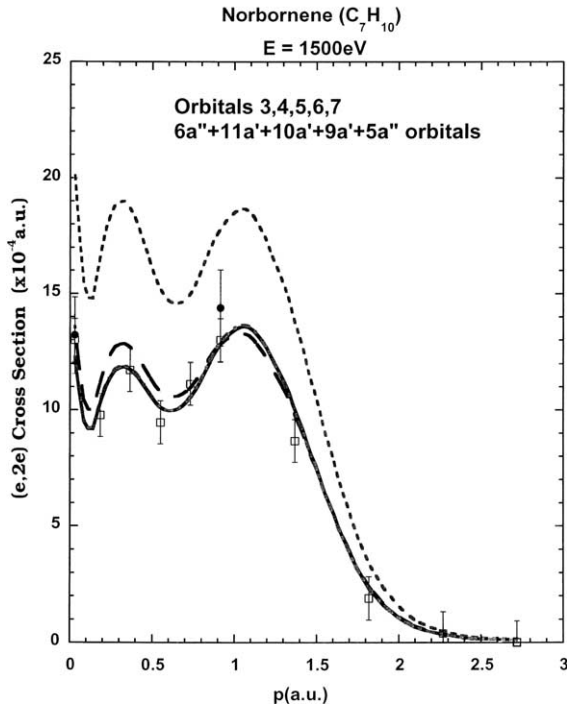

Fig. 2. The 1500 eV symmetric non-coplanar MD for the $6a'' + 11a' + 10a' + 9a' + 5a''$ orbitals of norbornene ($\varepsilon_f \sim 11.85$ eV). The present data for Run A (●) and Run B (□) are compared against the results of our PWIA-DFT calculations: (- - -) LSD/DZVP, (– –) LSD/TZVP, (—) BP/TZVP and (— - — -—) BLYP/TZVP. Note that in this case the BLYP/TZVP and BP/TZVP MD results are almost identical.

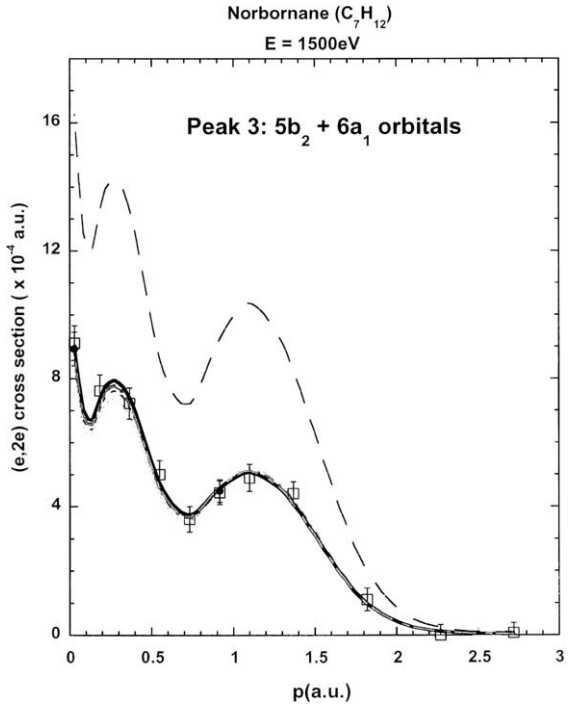

Fig. 3. The 1500 eV symmetric non-coplanar MD for the $5b_2+6a_1$ orbitals of norbornane ($\varepsilon_f \sim 11.6$ eV). The present data for Run A (●) and Run B (□) are compared against the results of our PWIA-DFT calculations: (- - -) BP/DZVP, (– –) BLYP/DZVP, (· - - - ·) BP/DZVP2, (···) BLYP/DZVP2, (—) BP/TZVP and (- —) BLYP/TZVP. Note that in this case the BLYP/TZVP and BP/DZVP2 MD results are very similar.

for the $5b_2+6a_1$ orbitals of norbornane. This MD was chosen as it illustrates nicely the general conclusions we can draw from norbornane when a comprehensive comparison is made for all its orbitals between the measured and calculated MDs. It is clear from Fig. 3 that the PWIA-BLYP/DZVP computation significantly overestimates the magnitude of the measured MD for all $p \leq 2.2$ a.u. It is also clear (although not as spectacularly in this case) that the PWIA-BLYP/DZVP2 calculation somewhat underestimates the magnitude of the cross-section for $0.1 < p$ (a.u.) < 0.7. On the other hand, the PWIA-BLYP/TZVP MD is in good agreement with the measured MD. These results illustrate that for norbornane a TZVP basis is superior to either DZVP or DZVP2. They also illustrate that here the BP GGA exchange-correlation functional is superior to the BLYP GGA exchange-correlation functional. This latter statement follows because PWIA-BP/DZVP and PWIA-BP/DZVP2 are in better agreement with the measured MD than either of the corresponding BLYP results.

We can therefore surmise that one of the most significant results from our EMS study into the chemically similar molecules NBD, NBN and NBA is that at least a TZVP basis quality is necessary in order to obtain an 'optimum' representation of the respective molecules. We now use this result in the extensive electronic structural calculations for these molecules that we have undertaken and now present.

4. Challenges to crystallographic experiments and existing theoretical studies of the species

Experimental crystallography measurements on the structural determination of these species are challenging tasks. It is known that electron diffraction (ED) and powder X-ray diffraction (XD) experiments serve as important molecular structural measurement means. In these experiments, even for most molecules of interest, it is not possible to determine the molecular structures completely, accurately and unambiguously from the intensities obtained from the ED or XD experiments alone [19]. For example, the $C_{(2)}$–$C_{(7)}$ distance of NBA from an XD experiment is unrealistically short (1.942 Å) [4], whereas the overestimation of the dihedral angle β between planes $C_{(1)}$–$C_{(2)}$=$C_{(3)}$–$C_{(4)}$ and H–$C_{(2)}$=$C_{(3)}$–H by a synchrotron X-ray study reflects the difficulties of accurately defining hydrogen positions from powder XD data [2]. Gas-phase electron diffraction (GED) and microwave (MW) experiments, on the other hand, depend critically either on the vibrational amplitudes [1] that are used in the GED analysis, or on the appropriate corrections in order to take account of inharmonicity on the assumption of harmonic vibration–rotation interactions [20]. Even though the GED experiment of NBA, when combined with other experiments such as MW, IR, Raman and some low-level ab initio calculations, gives a $C_{(1)}$–$C_{(2)}$ bond length of 1.536 Å and a $C_{(1)}$–$C_{(7)}$ bond length of 1.546 Å, it is still not possible to be confident whether the $C_{(1)}$–$C_{(2)}$ bond of NBA (in its ground electronic state) is longer or shorter than the $C_{(1)}$–$C_{(7)}$ bond [20]. As none of the experimental techniques can be used as a 'stand alone' technique to reveal the comprehensive structural information of the species, some work also attempts to augment the available procedures (MW, Raman and IR, etc.) with complementary experimental data [20]. However, as these different experiments have their own instrumental errors and data analysis processes, it can also be an important issue to ensure that the complementary experiments have sufficient consistency to give reliable and accurate results.

One also needs to consider the way in which the raw crystallographic data were analyzed, e.g. thermal motions and least-squares refinement, etc. The least-squares refinement technique is employed in many of the experiments to analyze signals obtained. This technique usually makes certain assumptions/constraints, such as in the NBA case where all the C–H bonds are assumed to be of the same length [4]. This constraint is not always a good approximation since not all the C–H bonds in the molecule are identical: they vary with the structural environment within the molecule, such as the bonding nature of the carbon atoms in the C–H bonds. Moreover, experimental results alone occasionally can be misleading due to matrix effects [21]. For example, it was concluded in some electron spin resonance (ESR) studies of the NBA cation radical species that the cations trapped in a variety of halocarbon matrices [22] led to an artificial C_s symmetry, with a long-bond

structure for the NBA cation radical [21]. Finally we note that some divergence between the experimental values and theoretical data should be expected, since theoretical data are obtained from the equilibrium states of the species, whereas the experiments, depending on their nature, give some type of vibrationally averaged values.

There have been some theoretical studies on NBD, NBN and NBA [1,19,23,24,25]. These earlier works provided additional structural information to the experiments and built up some confidence for the experimental structural determination. However, these studies either used rather low levels of theory such as HF/3-21G [1], empirical methods like molecular mechanics (MM) [19] or focused on other aspects of the molecules rather than their detailed structures, due to the limitations in the computing resources available [21]. Until the late 1980s, the 'seven heavy atom' framework had been considered too large for systematic ab initio investigations [1]. In the case of NBD for example it had been studied previously by a few semi-empirical approaches [26], and the ab initio CASSCF and CASCI calculations [27] which tried to predict the electronic spectrum of NBD. Subsequently little effort has been made to investigate the structure related property changes to the seven-membered carbon ring frame, in particular on the detailed structural and property changes of NBD, NBN and NBA as a result of C=C double bond saturation.

A systematic, higher level ab initio and DFT study focusing on the structural information of NBD, NBN and NBA is needed to reveal their bonding mechanism, and how their significant property differences stem from their subtle electronic structural differences. This paper therefore additionally provides such a study for these structurally resembled bicyclic hydrocarbons in their ground electronic states. In particular, we will investigate the effects on the seven-membered carbon skeleton as the C=C double bonds of NBD are replaced by C–C single bond (NBN) and two single C–C bonds (NBA). How these changes effect the nature and properties of the respective species, as well as the structural information of NBN which is responsible for the exo-selectivity of that species are also considered. The structure of the remainder of the present paper is as follows. Molecular orientation of the carbon skeleton, the carbon numbering scheme and a brief description of the computational details are given in Section 5. In Sections 6–8 results are presented and discussed in detail on a molecule by molecule basis. Section 9 compares the similarities and differences in the electronic structures of these species. Finally, conclusions drawn from the present work are given in Section 10.

5. Molecule orientation in space and computational details

Molecule orientation and symmetry are an essential part of molecular spectroscopy. The presence or absence of symmetry has consequences on the appearance of spectra, the relative reactivity of groups, and many other aspects of chemistry including the way that molecular orbitals and interactions are presented [28]. The bicyclic seven-carbon skeleton is orientated in a Cartesian coordinate system and the carbon atom numbering scheme is given in Fig. 4. The seven-carbon skeleton numbering starts from the carbon atom connecting both rings and moves anti-clockwise through the six-membered ring. The species are orientated in a way such that the methano carbon $C_{(7)}$ atom and its attached two hydrogen atoms lie in the *xz*-plane of the Cartesian coordinate system. The *y*-axis coincides with the line connecting atoms $C_{(1)}$ and $C_{(4)}$, and in parallel with the $C_{(2)}$–$C_{(3)}$ and $C_{(5)}$–$C_{(6)}$ bonds; whereas the *x*-axis is perpendicular to those C–C bonds. In the case of NBN, the double bond is the $C_{(2)}$–$C_{(3)}$ bond.

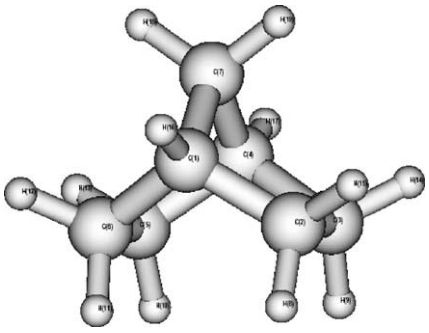

Fig. 4. The molecular orientation of the seven-member carbon skeleton.

The bridge ($C_{(1)}C_{(7)}C_{(4)}$) of the bicyclic carbon skeleton is known as the methano bridge whereas the six-membered ring is the so-called ethano ring. In the carbon skeleton, angle $\angle C_{(1)}C_{(7)}C_{(4)}$ is called the bridge angle, which links to the single bonded carbon $C_{(7)}$ (methano carbon), whereas $\angle HC_{(7)}H$, together with angles $\angle HC_{(5)}H$ and $\angle HC_{(6)}H$ in NBN and all $\angle HC_{(2)}H$, $\angle HC_{(3)}H$, $\angle HC_{(5)}H$ and $\angle HC_{(6)}H$ in NBA are called flap angles [4]. All those flap $\angle HCH$ angles, except for the $\angle HC_{(7)}H$ angle, are positioned on the ethano ring. Hydrogen atoms of the flap angles in the bridge side are called exo-Hs (or H_{exo}) and those towards the other side of the bridge are called endo-Hs (or H_{endo}) [1]. In NBN the H atom, which forms the $\angle HC_{(7)}H$ angle and points to the $C_{(5)}$–$C_{(6)}$ single bond, is called H_a (asymmetric), while the other H atom is therefore symmetric to the C=C bond and is called H_s [29]. It is noted that strained structures [25] contain atoms with bond angles departing from the standard bond angles of 109.47 and 120.00°, with respect to sp^3 and sp^2 hybrid carbon orbitals. As a result, more strain is expected if the bond angles significantly depart from their corresponding idealised hybridized carbon angles.

All our later (Sections 6–9) ab initio and DFT electronic calculations are carried out using both the GAMESS02 [30] and GAUSSIAN03 [31] suites of programs. For the ab initio calculations, all structures were optimized using restricted Hartree–Fock (RHF) and second order Moller–Plesset (MP2) levels of theory with respect to the 6-31G** [32]

and the GAMESS TZVP basis sets [33–35]. These were then followed by single point calculations at the optimized geometries with the given models. For example, either RHF/6-31G**//RHF/6-31G** or MP2/TZVP//MP2/TZVP (Single Point Calculation//Optimization) and so on. Similarly, the DFT calculations were performed using BLYP/BS//BLYP/BS and B3LYP/TZVP//B3LYP/TZVP models. Here, BS indicates the basis sets used, i.e. 6-31G** and TZVP, respectively. Molecular point group symmetries of the species are imposed in the electronic calculations, that is, the atoms are grouped by their irreducible representations and within the same symmetry representation. Under these circumstances the identical atoms and their bonds can be simply produced by symmetry.

6. Molecular electronic structural analysis for NBD

Norbornadiene (NBD, C_7H_8) in its ground electronic state (X^1A_1) is a closed shell molecule with 25 doubly occupied molecular orbitals (MOs), including 7 core MOs and 18 valence MOs. This molecule is very symmetric with two non-conjugated C=C bonds and a C_{2v} point group symmetry. In order to reveal the structural details, Fig. 5 provides three two-dimensional (2D) views of the optimized geometry of NBD with (i) being the birds-eye view of the *xy*-plane and (ii) and (iii) being side views of the projections on the *xz*-plane and *yz*-plane, respectively. Clearly, there exists a C_2-rotational axis as the principle axis (*z*-axis) of NBD and the bridge carbon $C_{(7)}$ atom locates on the *z*-axis. The carbon atoms in the methano bridge, i.e. $C_{(1)}$, $C_{(7)}$ and $C_{(4)}$, together with the two hydrogen atoms connecting to $C_{(1)}$ and $C_{(4)}$, are all confined in the *yz*-plane.

The total electronic energy of NBD using the RHF/6-31G** model (−269.666160 E_h) in the present study compares favourably with the energy of −269.659667 E_h using the RHF/6-31+G(d) model [24]. The fact that the total electronic energy of this species is −0.18 eV lower indicates that to polarize the hydrogen basis functions is more important to the energy than to use a diffuse function on the carbon atoms. In the present work, the RHF/TZVP model yields lower total electronic energy (−269.731477 E_h) than the RHF/6-31G** model (−269.666160 E_h). This result when coupled with those for the orbital momentum densities in Section 3, means that the discussion in this work will be mainly based on the calculations using the TZVP basis set. Table 1 presents our MP2/TZVP and B3LYP/TZVP calculation results, and other available theoretical and experimental geometric data, for the NBD ground electronic state (X^1A_1). In general our results from both the MP2/TZVP and B3LYP/TZVP calculations are consistent with those from the available experiments, for the C–C bond lengths and ∠CCC bond angles, with the discrepancies being within the experimental errors. This indicates that the MP2 and B3LYP methods are able to provide reliable and accurate results for this species and the following discussion will, therefore, focus on the results generated by the MP2/TZVP//B3LYP/TZVP calculations.

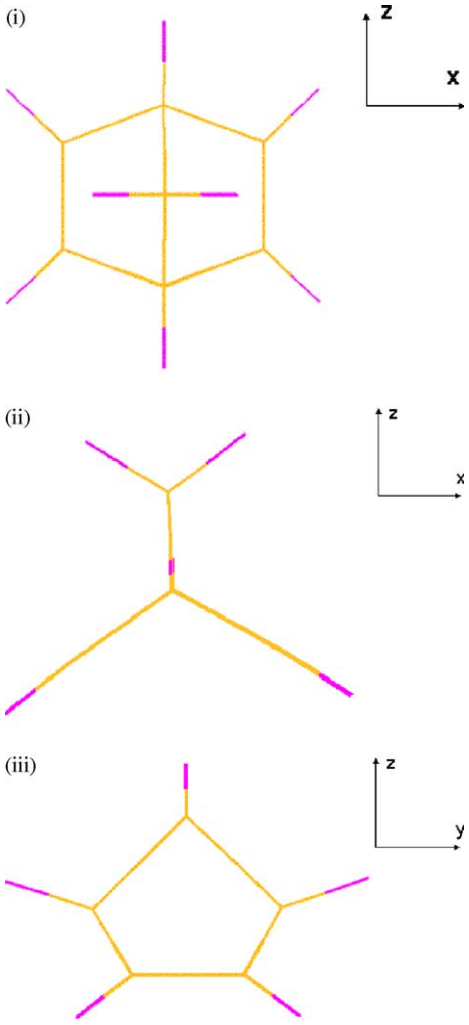

Fig. 5. Two-dimensional views of the bicyclic carbon skeleton of NBD (C_{2v} geometry), based on our RHF/TZVP calculations. (i) 'Birds-eye" view of the *xy*-plane, (ii) side view of the *xz*-plane and (iii) side view of the *yz*-plane.

The CC bond lengths of NBD are in the order: $r_{C=C} < r_{-C-C=} < r_{C-C}$, e.g. $C_{(2)}$–$C_{(3)}$ < $C_{(1)}$–$C_{(2)}$ < $C_{(1)}$–$C_{(7)}$. This order for the bond lengths is confirmed by MW [36] and ED experiments [4], as given in Table 1. Bond lengths for the two types of C–C single bond are not the same due to their different bonding mechanisms. Namely the strained sp^3–sp^3 single bonds, such as $C_{(1)}$–$C_{(7)}$ of 1.554 Å, are ∼0.021 Å longer than the sp^2–sp^3 single bond of $C_{(1)}$–$C_{(2)}$ (MP2/TZVP). The H atoms joined to those C atoms have bond lengths 1.079 and 1.090 Å for the $C_{(2)}$ (sp^2)–H and the $C_{(7)}$ (sp^3)–H bonds, respectively, whereas the three-way strained bridge $C_{(1)}$–H is 1.086 Å, half-way between the bond lengths of the C(sp^2)–H and the two-way strained $C_{(7)}$–H bonds. The flap $C_{(7)}$–H on the methano bridge yields the longest C–H bond length amongst the C–H bonds, while with C being a member of a double bond, such as the $C_{(2)}$–H bond, yields the shortest.

Table 1
Comparison of the molecular structure of norbornadiene (NBD, C_7H_8), electronic ground state (X^1A_1), with other theoretical work and experiments

Geometrical parameters	This work		Other work			Expt		
	MP2/TZVP	B3LYP/TZVP	HF [1]	MP2 [26]	HF [1,48]	MW [36]	ED [4]	XSCD[a] [38]
			STO-3G	6-31G*	3-21G			
$r(C_1–C_2)$/Å	1.533	1.543	1.548	1.540	1.550	1.530	1.533	1.536
$r(C_1–C_7)$/Å	1.554	1.560	1.556	1.551	1.566	1.557	1.571	1.555
$r(C_2–C_3)$/Å	1.344	1.333	1.311	1.319	1.319	1.336	1.339	1.337
$r(C_1–H)$/Å	1.086	1.088	1.007	–	1.076	1.090	1.109	–
$r(C_2–H)$/Å	1.079	1.081	1.088	–	1.069	1.081	1.090	–
$r(C_7–H)$/Å	1.090	1.091	1.087	–	1.081	1.095	1.109	–
$\angle(C_1C_2C_3)$°	107.026	107.172	107.4	–	107.5	107.13	–	107.2
$\angle(C_1C_7C_4)$°	92.327	91.977	91.9	91.87	92.0	91.90	92.2	92.5
$\angle(C_2C_1C_6)$°	107.675	107.336	106.5	107.45	106.2	107.58	–	106.9
$\angle(C_2C_1C_7)$°	98.257	98.312	98.4	98.31	98.3	98.30	–	98.3
$\angle(C_7C_1H)$°	117.782	117.886	118.1	–	118.2	117.66	–	–
$\angle(C_3C_2H)$°	127.668	128.141	128.8	–	128.1	127.84	125.2	–
$\angle(HC_7H')$°	111.024	110.957	109.0	–	111.7	111.99	114.7	–

[a] Laboratory X-ray single crystal study at 110 K.

The two-way strained methano bridge angle ($\angle C_{(1)}C_{(7)}C_{(4)}$) is 92.327° in the present work, which is in excellent agreement with the experimental value of 92.2 ± 0.3° (see Table 1). This angle is −17.14° strained from the idealized 109.47° of the hybridized sp^3–sp^3 carbon–carbon bond. As a result of this strain, the flap angle of $\angle HC_{(7)}H'$, given by the present calculations as 111.024°, is 1.554° flatter from the optimal angle of 109.47°. The present calculations of these angles are in excellent agreement with the MW experiment result of 111.99° [36], whereas the flap angle of NBD given by the ED experiment (114.7°) [4] seems too large.

7. Methano ring in the carbon skeleton of NBN

Norbornene (C_7H_{10}) exhibits very different properties, such as its chemical reactivity and exo-selectivity. Its electronic structure must be responsible for these unique properties. Due to its C_s point group symmetry, the electronic ground state is X^1A', which has 26 doubly occupied MOs, including 7 core MOs and 19 valence MOs. The optimized molecular geometry of the molecule is reported in Table 2, together with results from other theoretical and experimental work. Fig. 6(i)–(iii) give 2D views of the NBN geometry. As the NBN molecule has only

Table 2
Comparison of the molecular structure of norbornene (NBN, C_7H_{10}), electronic ground state (X^1A'), with other theoretical work and experiments

Geometrical parameters	This work		Other work		Expt		
	MP2/TZVP	B3LYP/TZVP	HF [1]	HF [49]	ED [37]	XPD [38]	SRPD [2]
			STO-3G	4-31G(d)*			
$r(C_1–C_2)$/Å	1.512	1.530	1.535	1.524	1.529	1.524	1.524
$r(C_1–C_6)$/Å	1.561	1.582	1.563	1.564	1.550	1.562	1.558
$r(C_1–C_7)$/Å	1.538	1.560	1.548	1.547	1.566	1.547	1.543
$r(C_5–C_6)$/Å	1.552	1.573	1.556	1.559	1.556	1.556	1.560
$r(C_2–C_3)$/Å	1.348	1.349	1.314	1.334	1.336	1.334	1.332
$r(C_1–H)$/Å	1.087	1.095	1.087	1.078	–	–	–
$r(C_2–H)$/Å	1.081	1.099	1.081	1.070	1.103	–	–
$r(C_7–H)$/Å	1.089	1.088	1.087	1.082	–	–	–
$r(C_6–H_{exo})$/Å	1.089	1.096	1.087	1.083	–	–	–
$r(C_6–H_{endo})$/Å	1.091	1.098	1.087	1.081	–	–	–
$\angle(C_1C_2C_3)$°	107.34	107.59	107.8	108.0	108.6	106.5	108.1
$\angle(C_1C_6C_5)$°	102.87	102.80	102.9	–	–	100.5	103.5
$\angle(C_1C_7C_4)$°	93.60	93.62	93.3	93.5	–	92.3	95.3
$\angle(C_2C_1C_6)$°	106.26	106.36	106.4	105.9	–	109.3	105.6
$\angle(C_2C_1C_7)$°	100.28	100.21	99.4	–	–	102.1	99.6
$\angle(C_6C_1C_7)$°	100.13	100.18	100.9	–	–	99.4	99.0
$\angle(C_7C_1H)$°	117.16	116.91	113.3	–	114.1	–	–
$\angle(H_{exo}C_6H_{endo})$°	108.19	107.94	–	–	–	–	–
$\angle(H_sC_7H_a)$°	110.32	110.14	109.7	110.1	–	–	–

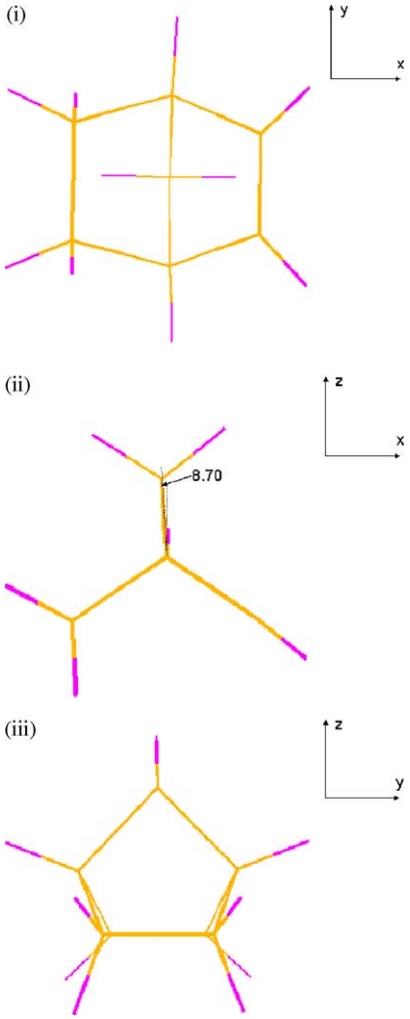

Fig. 6. Two-dimensional views of the bicyclic carbon skeleton of NBN (C_s geometry), based on our RHF/TZVP calculations. (i) 'Birds-eye' view of the *xy*-plane, (ii) side view of the *xz*-plane and (iii) side view of the *yz*-plane.

one C=C double bond, which causes a reduction in its molecular symmetry, NBN is more computationally demanding than NBD and more geometric parameters are required. The total electronic energy of NBN is given by −270.871149, −271.849717 and −272.626398 E_h, in this work using RHF/6-31G**, MP2/6-31G** and B3LYP/6-31G**, respectively, which are consistent with the results of −270.8618412, −271.8611977 and −272.7362679 E_h using the same methods with a 6-31+G* basis set [24]. Again, similar to what has been found in the NBD case, in the RHF calculations a polarization function added to the H atom basis set makes a more important contribution to lowering the total energy than an additional diffuse basis function to the C atom basis set.

The less symmetric NBN electronic structure in fact accounts for its unique molecular properties. Unlike NBD, the two single bonds, $C_{(1)}$–$C_{(2)}$ and $C_{(1)}$–$C_{(6)}$ of the NBN molecule are not equivalent anymore since the $C_{(2)}$ atom links to the C=C double bond and the $C_{(6)}$ atom relates to a C–C single bond in NBN. There are four types of non-equivalent C–C single bonds in NBN, namely, $C_{(1)}$–$C_{(2)}$, $C_{(1)}$–$C_{(6)}$, $C_{(5)}$–$C_{(6)}$, and $C_{(1)}$–$C_{(7)}$, which all stem from different bonding mechanisms (and cannot be produced by symmetry). The bond lengths of these C–C single bonds are evaluated in this work by the B3LYP/TZVP model as 1.521, 1.568, 1.561 and 1.543 Å, respectively, which are in excellent agreement with the corresponding values 1.524, 1.562, 1.556 and 1.547 Å from the ED experiment [37]. This trend also indicates that the C–C single bonds, which are engaged with a sp^2 carbon atom, such as the $C_{(1)}$–$C_{(2)}$ bond, are in general shorter than those engaged with sp^3 carbon atoms.

There is an apparent impact on the saturation of the NBD $C_{(5)}$=$C_{(6)}$ bond in NBN, as shown in Fig. 6. The fact that the $C_{(1)}$–$C_{(6)}$ bond is the second longest C–C single bond in NBN is consistent in both the ab initio and DFT calculations given in Table 2, and is also consistent with the results from the ED [4] and XPD [38] experiments. Saturation of the $C_{(5)}$=$C_{(6)}$ bond in NBD causes a shrinkage of the $C_{(1)}$–$C_{(2)}$ bond, from 1.533 Å in NBD to 1.512 Å in NBN (MP2/TZVP), a reduction of −0.021 Å in the bond length. However, such a C=C double bond saturation significantly elongates the $C_{(1)}$–$C_{(6)}$ single bond, from 1.533 Å in NBD to 1.561 Å in NBN, a bond expansion of 0.028 Å. Furthermore, there is also an impact on the $C_{(1)}$–$C_{(7)}$ bond, which is 1.554 Å in NBD, but shrinks to 1.538 Å in NBN, a change of −0.016 Å. Hence, it seems that the saturation of the NBD $C_{(5)}$=$C_{(6)}$ bond has a larger impact on the ethano ring than on the methano bridge of the NBN molecule, and also on the bonds which directly connect to one of the saturated carbon atoms rather than the indirectly connected carbon bonds.

The most important structural impact of the double bond saturation is that the methano bridge of $C_{(1)}$–$C_{(7)}$–$C_{(4)}$ in NBN is no longer confined in the same plane (the *yz*-plane) with H–$C_{(1)}$–$C_{(4)}$–H, as in both NBD and NBA (refer to Fig. 6(ii)). Instead, a dihedral angle in NBN, which is formed by the planes H–$C_{(1)}$–$C_{(4)}$–H and $C_{(1)}$–$C_{(7)}$–$C_{(4)}$, is calculated to be 8.70° by the RHF/TZVP model. This dihedral angle causes that the methylene $C_{(7)}H_2$ group in the methano bridge to tilt towards the single C–C bond side of $C_{(5)}$–$C_{(6)}$, and leads the molecule to completely lose the C_2-rotational axis. Such substantial structural changes suggest that the NBN skeleton predisposes it toward rapid reaction on the exo face of the double bond. As indicated in Figs. 5(ii) and 6(ii), the C–H olefinic bonds (C–H bonds on the sp^2 carbon atoms, i.e. $C_{(2)}$–H, $C_{(3)}$–H) of NBN are slightly bent endo (opposite to the bridge side), causing the π bonds of norbornene and norbornadiene to be chemically non-equivalent. For example, in our recent electron momentum spectroscopy (EMS) analysis of NBD [8,9] we demonstrated that the HOMO of NBD exhibits a p-electron dominant contribution to the π bond, whereas our most recent experimental and theoretical EMS analysis [39] of NBN indicates that the HOMO is significantly distorted and dominated by strong σ bonding characteristics.

This observation is in good agreement with the conclusion drawn by Inagaki et al. [40] using second-order-perturbation theory.

Nevertheless, NBN is more hindered on the endo face than the NBD molecule (also see Figs. 5(ii) and 6(ii)). As the non-zero dihedral angle of the methano bridge and the C–H olefinic bonds for NBN are bent endo, as indicated in Fig. 6(ii), the π system asymmetry and exo/endo stereoselectivity contribute to the reactivity of these species [41]. Attachment of radicals on NBN gives exo-addition as the major product (exo:endo = 99.5:0.5) [7], whereas NBD gives a mixture of exo and endo of 35–43:17–21:others [42]. Moreover, the out of plane deviation is almost doubled in NBN (β in Table 4 is 7.65° as given by MP2/TZVP) compared to that of NBD (3.33° from the same MP2 calculation), indicating that the repulsive interactions are reduced during the endo bending, but increased during the exo bending, so that exo-selectivity is more important to the reactivity of NBN than to NBD.

8. Saturated bicyclic hydrocarbon of NBA

The ground electronic state for fully saturated NBA is X^1A_1, and its 27 doubly occupied MOs consist of 7 core MOs and 20 valence MOs. A summary of our electronic structural calculations for the NBA ground state is given in Table 3. All the C–C bonds are strained single bonds in NBA. However, due to their different bonding mechanisms the respective bond lengths are quite different: the hydrogen saturated $C_{(2)}$–$C_{(3)}$ bond becomes the longest C–C bond while the bridge $C_{(1)}$–$C_{(7)}$ bond is the shortest according to both the present theoretical calculations and the ED experiment [4]. Nevertheless, since all the C–C bonds in NBA are single sp^3 bonds we might anticipate the C–H bond lengths to not exhibit much difference from one another. Under these circumstances it may be a good first approximation, in the least-squares fit of the experimental crystallographic intensities, that all the C–H bond lengths can be assumed to be the same (see Table 3) [4,43,20].

Accurate determination of the electronic structure of NBA provides the greatest challenge to crystallographic experiments amongst the three species. In Table 3 the electronic structure of NBA predicted by the present work, is compared with one of the available experimental results. All the theoretical structural information is consistent with respect to the C–C bond lengths, the C–H bond lengths and the $\angle$CCC angles. However, it seems that the available experimental structural data lacks some certain consistency, e.g. in the experimental trend of the three groups of C–C bonds in the molecule. Here, all the theoretical calculations consistently give the trends in the NBA C–C bond lengths as $C_{(1)}$–$C_{(7)} < C_{(1)}$–$C_{(2)} < C_{(2)}$–$C_{(3)}$. Unfortunately, the available experiments are not consistent with respect to that trend: that is, $C_{(2)}$–$C_{(3)} < C_{(1)}$–$C_{(7)} < C_{(1)}$–$C_{(2)}$ from SRPD [43], while $C_{(1)}$–$C_{(2)} < C_{(1)}$–$C_{(7)} < C_{(2)}$–$C_{(3)}$ from ED [4] and [20]. Moreover, the experimental C–H bonds of NBA seem unrealistically long (1.113 Å [20]), compared to the C–H bonds containing sp^3 C atoms in NBD and NBN. This may stem from the inappropriate constraint, in the least-squares fit, of assuming that all the C–H bond lengths in the NBA molecule are equivalent. Such an assumption neglects the non-equivalence of the bonds between the different symmetry groups due to their molecular environment. Furthermore, the experimental and theoretical angles among the atoms are generally in good agreement, except for the $\angle C_{(2)}C_{(1)}C_{(6)}$ of SRPD [43] which is 103.4°, some 5° smaller than most of the other studies in Table 3.

It is also noted that the different flap angles $\angle H_{exo}C_{(6)}H_{endo}$, which is in the ethano ring, and $\angle HC_{(7)}H'$, which is in the methano bridge, are assumed to be the same in the three crystallography experiments [43,4,20]. It seems

Table 3
Comparison of the present theoretical molecular structure of norbornane (NBA, C_7H_{12}), electronic ground state (X^1A_1), using DFT calculations, with other data

Geometrical parameters	DFT			Expt [20]
	BLYP/BS//BLYP/BS		B3LYP	
	6-31G**	TZVP	TZVP	
$r(C_1$–$C_2)$/Å	1.559	1.558	1.547	1.536
$r(C_1$–$C_7)$/Å	1.558	1.556	1.544	1.546
$r(C_2$–$C_3)$/Å	1.580	1.579	1.567	1.573
$r(C_1$–H)/Å	1.101	1.097	1.091	1.113
$r(C_2$–H)/Å	1.102	1.099	1.092	1.113
$r(C_7$–H)/Å	1.102	1.099	1.093	1.113
$\angle(C_1C_2C_3)$°	103.092	103.080	103.059	102.71
$\angle(C_1C_7C_4)$°	94.414	94.442	94.384	93.41
$\angle(C_2C_1C_6)$°	108.376	108.376	108.502	108.97
$\angle(C_2C_1C_7)$°	101.554	101.558	101.557	102.04
$\angle(C_7C_1H)$°	116.128	116.083	116.120	–
$\angle(H_{exo}C_6H_{endo})$°	107.286	107.417	107.260	107.2
$\angle(HC_7H')$°	109.026	109.174	109.039	107.2
E_{total}, $E_h(-272.0+)$	−1.80247	−1.883222	−1.860520	–

a reasonably good approximation to assume that all the ∠HCHs in the *ethano ring* are the same, and in fact they are identical angles that can be generated by the NBA molecular symmetry. However, it is obviously a poor approximation to assume that the flap angles ∠HCH in the ethano ring are the same as the flap angle $\angle HC_{(7)}H'$ in the methano bridge. This latter angle cannot be produced by symmetry from any flap angle in the ethano ring, since they are different angles by symmetry. The flap angle in the ethano ring $\angle H_{exo}C_{(6)}H_{endo}$ is 107.673° (MP2/TZVP) while the flap angle in the methano bridge $\angle HC_{(7)}H'$ is given by the same calculation as 109.275°. Nevertheless, the methano ring of NBA (with the $\angle C_{(1)}C_{(7)}C_{(4)}$ being ≈94°) is much more strained than its counterparts in the ethano ring (with the ∠CCC angles being ≈107°). Nonetheless our theoretical calculations, with their high accuracy and consistency, together with the existing crystallographic experimental data gives us confidence in the NBA electronic structural determination, as overall the agreement between them is good.

9. An electronic structural comparison of NBD, NBN and NBA

Norbornadiene, norbornene and norbornane have substantial electronic structures. If these three molecules orientate in the same Cartesian coordinate system as defined in Section 5, the correlation diagram for their irreducible representations is given by a_1, $b_1 \rightarrow a'$ and a_2, $b_2 \rightarrow a''$, when one of the C=C double bonds of NBD is saturated by H atoms or when one of the ethano single bonds of NBA becomes a C=C double bond. In both scenarios the resulting structure becomes that of the NBN, a species with the lower symmetry C_s. The 2D structural views of these species, given in Figs. 5–7, highlight the structural differences for NBD, NBN and NBA, respectively. Figs. 5 and 7 provide 2D views of NBD and NBA, both with C_{2v} point group symmetry. There clearly exists a C_2-rotational axis as the principle axis (*z*-axis) and the bridge carbon $C_{(7)}$ locates on the *z*-axis. The carbon atoms in the methano bridge, i.e. $C_{(1)}$, $C_{(7)}$ and $C_{(4)}$, together with the two hydrogen atoms connecting to $C_{(1)}$ and $C_{(4)}$, are all confined in the *yz*-plane in both NBD and NBA. The two halves of the six-carbon ring of NBD and NBA, divided by the σ_{yz} plane, are identical and can be produced by their molecular symmetry. The most important difference in the NBN species, as shown in Fig. 6, is the reduction of such a symmetry which causes the position of bridge carbon $C_{(7)}$ to be located out of the *yz*-plane and in fact not even on the *z*-axis. As a result a dihedral angle of 8.70°, between planes $H_{(8)}$–$C_{(1)}$–$C_{(4)}$ and $C_{(1)}$–$C_{(7)}$–$C_{(4)}$, is produced by the symmetry reduction in NBN. The fact that the methano bridge tilts to the opposite side of the C=C bond of NBN was also indicated by Ohorodnyk and Santry [44]. However, many structural diagrams of NBN are misleading: the methylene group of $C_{(7)}H_2$ is usually presented in a way that the methano carbon $C_{(7)}$ incorrectly tilts to the C=C bond [4].

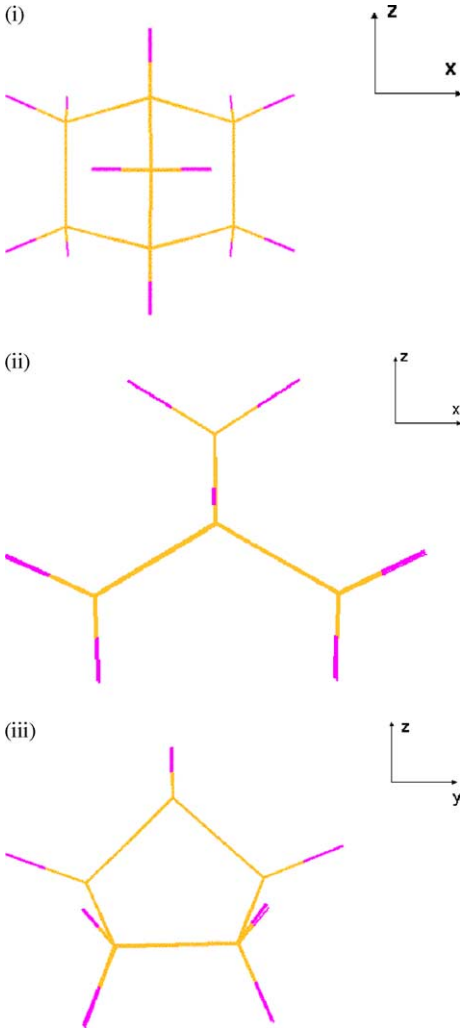

Fig. 7. Two-dimensional views of the bicyclic carbon skeleton of NBA (C_{2v} geometry), based on our RHF/TZVP calculations. (i) 'Birds-eye' view of the *xy*-plane, (ii) side view of the *xz*-plane and (iii) side view of the *yz*-plane.

There are three types of CC bonds involved in these species, i.e. C=C double bonds (e.g. $C_{(2)}$–$C_{(3)}$, for NBD and NBN), strained C–C single bonds (e.g. $C_{(1)}$–$C_{(7)}$) and –C–C= single bonds (e.g. $C_{(1)}$–$C_{(2)}$, NBN), which associates with three types of C–H bonds due to the unique atom groups in the molecules. Table 4 provides a summary of our electronic structural calculations for NBD, NBN and NBA, using the MP2/TZVP and B3LYP/TZVP models as well as the available experiments. This Table also clearly shows trends and structural properties in these species as a consequence of the saturation of the C=C double bond(s) of NBD and NBN by hydrogen atoms. In general, the C–H bonds with the C atom being a part of a C–C single bond have longer bond lengths than the corresponding bonds with their C atom being a part of a double bond; similarly the C–H bonds in the methano bridge are longer than their counterparts in the ethano ring (except for $C_{(6)}$–H in NBN).

Table 4
Comparison of the NBD, NBN and NBA structures as the C=C double bonds are saturated

Geometrical parameters	MP2/TZVP//MP2/TZVP			B3LYP/TZVP//B3LYP/TZVP			Expt		
	NBD	NBN	NBA	NBD	NBN	NBA	NBD	NBN	NBA
$r(C_1–C_2)$/Å	1.533	1.512	1.538	1.543	1.521	1.547	1.536	1.524	1.536
$r(C_1–C_7)$/Å	1.554	1.538	1.535	1.560	1.547	1.544	1.555	1.543	1.546
$r(C_5–C_6)$/Å	–	1.554	–	–	1.561	–	–	1.560	–
$r(C_2–C_3)$/Å	1.344	1.348	1.558	1.333	1.338	1.567	1.337	1.332	1.573
$C_2\cdots C_7$/Å	2.335	2.341	(2.379)	2.348	2.354	(2.395)	–	2.302	–
$C_6\cdots C_7$/Å	(2.335)	2.376	2.379	(2.348)	2.391	2.395	–	–	–
$r(C_1–H)$/Å	1.086	1.087	1.089	1.088	1.089	1.091	–	–	–
$r(C_2–H)$/Å	1.079	1.081	1.091	1.081	1.082	1.092	–	–	–
$r(C_7–H)$/Å	1.090	1.089	1.091	1.091	1.091	1.093	–	–	–
$r(C_6–H)$/Å	–	1.089	–	–	1.091	–	–	–	–
$r(C_6–H')$/Å	–	1.091	–	–	1.092	–	–	–	–
$\angle(C_1C_2C_3)^\circ$	107.026	107.340	103.182	107.172	107.562	103.059	107.2	108.1	102.71
$\angle(C_1C_6C_5)^\circ$	–	102.869	–	–	102.778	–	–	103.4	–
$\angle(C_1C_7C_4)^\circ$	92.327	93.598	94.596	91.977	93.606	94.414	92.5	95.3	93.41
$\angle(C_2C_1C_6)^\circ$	107.675	106.261	108.568	107.336	106.372	108.376	106.9	105.6	108.97
$\angle(C_7C_1H)^\circ$	117.782	117.162	116.170	117.886	116.977	116.128	–	–	–
$\angle(HC_6H')^\circ$	–	108.193	107.63	–	107.649	107.417	–	–	–
$\angle(HC_7H')^\circ$	111.024	110.302	109.275	110.957	109.919	109.206	–	–	–
$\beta^{a\circ}$	3.33	7.65	–	3.76	6.46	–	12.0[b]	4.5	–
E_{total}/E_h	−270.722392	−271.953390	−273.175530	−272.626398	−271.383652	−273.860520	–	–	–

[a] Here the angle β is the smaller dihedral angle $C_1–C_2–C_3–H$.
[b] The rather high value of the experimental β angle reflects the diffculties of accurately defining hydrogen positions from powder X-ray diffraction data [2].

If only single bonds are in the system, such as those in NBA, the C–H bonds with the C atoms being the bridge C atoms (i.e. $C_{(1)}$ and $C_{(4)}$) possess the shortest C–H bonds.

The bonds of $C_{(1)}$–$C_{(2)}$ and $C_{(1)}$–$C_{(7)}$ remain as single bonds in all three species. The $C_{(1)}$–$C_{(2)}$ bond of NBD is 1.533 Å and it shrinks to 1.512 Å in NBN, as the $C_{(5)}$–$C_{(6)}$ double bond is saturated. This bond is, however, significantly elongated from 1.512 Å in NBN to 1.538 Å to give NBA, when the last C=C double bond is saturated. On the other hand, the change in the $C_{(1)}$–$C_{(2)}$ bond length is subtle as the two double C=C bonds of NBD are saturated simultaneously to give NBA, increasing by only 0.005 Å. This also indicates that the $C_{(1)}$–$C_{(2)}$ bond length responds to the changes in the C=C double bond significantly, as the molecular species interchanges between C_{2v} and C_s point group symmetry. It does not alter much as long as the molecular point group symmetry remains as C_{2v} while undergoing bond nature changes, i.e. this ($C_{(1)}$–$C_{(2)}$) bond length only experiences small variations when both of the double C=C bonds of NBD are saturated by the H atoms. This is because the C_{2v} symmetry is able to balance the forces caused by the lower symmetry structure. The single $C_{(1)}$–$C_{(7)}$ bond on the methano bridge is also not affected dramatically by such a C=C saturation or changes in the molecular point group symmetry. The C_1–C_7 bond shrinks when the $C_{(5)}$–$C_{(6)}$ C=C bond of the NBD saturates to give NBN, but this bond does not have significant variation when the second C=C double bond, i.e. $C_{(2)}$–$C_{(3)}$ is saturated. Consequently, the impact of the saturation of the C=C double bonds on the $C_{(1)}$–$C_{(2)}$ single bond length (the ethano ring) is more significant than that on the $C_{(1)}$–$C_{(7)}$ bond length (methano bridge).

The related C–H single bond lengths reflect indirectly such a fact with only small changes in the C–C bonds they are attached to. For example, like the $C_{(1)}$–$C_{(7)}$ bond, the $C_{(1)}$–H and $C_{(7)}$–H bonds do not vary significantly when the number of C=C double bonds alter. Specifically, the $C_{(1)}$–H bond length is 1.086, 1.087 and 1.089 Å in NBD, NBN and NBA, respectively (see Table 4). Similarly, the $C_{(7)}$–H bond is consistent with the same conclusion, i.e. the $C_{(7)}$–H bond length is 1.090, 1.089 and 1.091 Å for NBD, NBN and NBA, respectively. However, the $C_{(2)}$–H bond length is more sensitive to the structural changes of the C=C double bonds because of the associated changes in the bond order. It is 1.079, 1.081 and 1.091 Å for NBD, NBN and NBA, respectively. Such changes in this bond length reflect the bond order of the carbon atoms which the C–H bonds attach to.

The bond angles, however, react to the C=C bond saturation quite differently. The $\angle C_{(1)}C_{(2)}C_{(3)}$ increases slightly (0.214°) between NBD and NBN, but has a large decrease of 4.158° when NBN becomes NBA. This effect is because the $C_{(1)}$–$C_{(2)}$ and $C_{(2)}$=$C_{(3)}$ bonds in $\angle C_{(1)}C_{(2)}C_{(3)}$ remain unchanged as single and double bonds, respectively, in both NBD and NBN. However, this bond changes significantly to become a single $C_{(2)}$–$C_{(3)}$ bond length, and a larger $\angle$CCC bond angle change is therefore expected. Moreover, it is also noted that when all the C=C double bonds are saturated, the ethano ring of the seven-membered carbon skeleton becomes less strained (the bond angles are closer to the hybridized carbon angles), as does the methano bridge.

The bridge angle $\angle C_{(1)}C_{(7)}C_{(4)}$ in the methano ring has a steady increase of approximately 1.0° when NBD is converted to NBN and then to NBA, towards the direction of less strain and therefore a more stable structure. This is because when the C=C bonds are saturated the corresponding single C–C bonds exhibit longer bond lengths, as demonstrated in Fig. 6(i) and (iii) by the two non-equivalent bonds in NBN. The $\angle C_{(2)}C_{(1)}C_{(6)}$ angle experiences changes of a very different nature: there is a 1.414° shrinkage when the first double bond $C_{(5)}$–$C_{(6)}$ of NBD is saturated to give NBN, whereas this angle has a 2.307° increase when the last C=C bond in NBN saturates to give NBA. Finally, the flap angle $\angle HC_{(7)}H'$ shrinks from 111.024° in NBD to 110.302° in NBN and then to 109.275° in NBA, that is, the bond angle is relaxed towards the optimum angle of 109.47°, i.e. becomes less strained.

As indicated in the previous sections the most important structural change amongst the three species is the dihedral angle being split from the *yz*-plane in NBN, as a result of the molecular symmetry reduction. Such a dihedral angle of 8.70° indicates that NBN possesses some unique properties such as strong chemical reactivity and a larger dipole moment than its more symmetric counterparts NBD and NBA. This follows as the tilting of the $C_{(7)}H_2$ group in the methano bridge makes the $C_{(2)}$=$C_{(3)}$ bond more exposed in space for other agents to attack from the exo-side in chemical reactions. Moreover, due to its lower symmetry, the dipole moment of NBN = 0.327 debye [4] is many times larger than either NBD = 0.05866 debye [4] or NBA = 0.09 debye [45].

10. Conclusions

We have reported on some of our results from our EMS studies into the respective valence electronic structures of NBD [8,9], NBN and NBA. On the basis of a detailed comparison between our calculated and measured orbital momentum densities, for each molecule, we found that the optimum (but not perfect) representation of said species was provided by the TZVP basis set. This result was then used in our detailed structural calculations that followed.

Highly accurate, unambiguous and conclusive ab initio and DFT calculations for the electronic structure on the ground electronic states of norbornadiene (C_7H_8, NBD), norbornene (C_7H_{10}, NBN) and norbornane (C_7H_{12}, NBA) have also been provided along with detailed a structural analysis. All our calculations are generally consistent and provide structural insight into the similarities and differences between the molecules. The structural parameters

of the three species obtained in the present work, using a TZVP basis set, agree well with available crystallographic measurements and could stand alone as an independent source of information to build confidence when the crystallographic experimental results become ambiguous.

This study focused on the molecular electronic structural changes and trends that occur as a result of the C=C double bonds being saturated by hydrogen atoms. It was found that there is a general trend that the three molecules try to relax the strains on both of the ethano and methano rings, via the structural changes, whenever this is possible. As the ethano ring directly contains the C=C bonds which are being saturated, the structural parameters of the ethano ring exhibited more significant changes than those in the methano bridge, as expected. The present study provides particularly useful information for the structure of the NBA molecule. Our theoretical predictions on its structure are able to provide assistance and reference for the crystallography experiments, as well as to improve the model or constraints employed in the least-squares-fit procedures. For example, in assuming the same bond length for the C–H bonds by their symmetry, not simply by their attachment to the single C–C bonds.

The most important contribution of the present calculations is to indicate that there exists a dihedral angle of 8.70° in NBN, between the methano bridge and the Cartesian *yz*-plane, due to its asymmetric electronic structure. It is this dihedral angle in NBN, which significantly reflects the symmetry reduction in NBN and contributes to its chemical reactivity and other properties, which are obviously different from NBD and NBA. Consequently, the three species are compounds with substantially different electronic structures.

Acknowledgements

The authors acknowledge the Australian Partnership for Advanced Computing (APAC) for using the Compaq SC Alphaserver Cluster National Facilities. One of the authors (FW) would like to acknowledge useful discussions with Dr Harry Quiney, while we all would like to thank Ms Kate Nixon for her assistance on the literature survey. Finally, MJB thanks the organising committee of Sagamore XIV for supporting his attendance at that meeting.

References

[1] C.R. Castro, R. Dutler, A. Rauk, H. Wieser, J. Am. Chem. Soc. 90 (1968) 3149.
[2] M. Brunelli, A.N. Fitch, A. Jouannaux, A.J. Mora, Z. Kristallogr. 216 (2001) 51.
[3] T.P. Nevell, E. DeSakas, C.L. Wilson, J. Phys. Soc. 1939; 1188.
[4] J.F. Chiang, C.F. Wilcox Jr., S.H. Bauer, J. Mol. Struct. (Theochem) 165 (1987) 241.
[5] J. Spanget-Larsen, R. Gleiter, Tetrahedron Lett. 23 (1982) 2435.
[6] A.J.G. Barwise, A.A. Gorman, M.A.J. Rodgers, Chem. Phys. Lett. 38 (1976) 313.
[7] N. Koga, T. Ozawa, K. Morokuma, J. Phys. Org. Chem. 3 (1990) 519.
[8] H. Mackenzie-Ross, M.J. Brunger, F. Wang, W. Adcock, N. Trout, D.A. Winkler, J. Elec. Spectrosc. Relat. Phenom. 123 (2002) 389.
[9] H. Mackenzie-Ross, M.J. Brunger, F. Wang, W. Adcock, T. Maddern, W.R. Newell, I.E. McCarthy, E. Weigold, B. Appelbe, D.A. Winkler, J. Phys. Chem. A 106 (2002) 9573.
[10] M.J. Brunger, W. Adcock, J. Chem. Soc., Perkin Trans. 2 (2002) 1.
[11] E. Weigold, I.E. McCarthy, Electron Momentum Spectroscopy, Kluwer Academic/Plenum Publishers, New York, 1999.
[12] G. Bieri, F. Burger, E. Heilbronner, J.P. Maier, Helv. Chim. Acta 60 (1977) 2213.
[13] P. Bischof, J.A. Hashmall, E. Heilbronner, V. Harnung, Helv. Chim. Acta 52 (1969) 1745.
[14] M. Getzlaff, G. Schönhense, J. Elec. Spectrosc. Relat. Phenom. 95 (1988) 225.
[15] P.R. Bevington, D.K. Robinson, Data Reduction and Error Analysis for the Physical Sciences, McGraw-Hill, New York, 1990.
[16] W. Kohn, L.J. Sham, Phys. Rev. A 140 (1965) 1133.
[17] M.T. Michalewicz, M.J. Brunger, I.E. McCarthy, V.M. Norling, in: R. Shaginaw (Ed.), CRAY Users Group 1995 Fall Proceedings, Alaska (1995), pp. 37–41.
[18] I.E. McCarthy, E. Weigold, Rep. Prog. Phys. 54 (1991) 789.
[19] N.L. Allinger, H.J. Geise, W. Pyckhout, L.A. Paquette, J.C. Gallucci, J. Am. Chem. Soc. 111 (1989) 1106.
[20] L. Doms, L. van der Enden, H.J. Geise, C. van Alsenoy, J. Am. Chem. Soc. 105 (1983) 158.
[21] M.J. Shephard, M.N. Paddon-Row, J. Phys. Chem. 99 (1995) 3101.
[22] M. Okazaki, K. Toriyama, J. Phys. Chem. 97 (1993) 8212.
[23] N. Bodor, M.J.S. Dewar, S.D. Worley, J. Am. Chem. Soc. 92 (1970) 19.
[24] R.R. Sauers, Tetrahedron 54 (1998) 5143.
[25] C.-Y. Zhao, Y. Zhang, X.-Z. You, J. Phys. Chem. A 101 (1997) 5174.
[26] M.Z. Zgierski, F. Zerbetto, J. Chem. Phys. 98 (1993) 14.
[27] B.O. Roos, M. Merchan, R. McDiarmid, X. Xing, J. Am. Chem. Soc. 116 (1994) 5927.
[28] A. Rauk, Orbital Interaction Theory of Organic Chemistry, second ed., Wiley, New York, 2001.
[29] R. Abraham, J. Fisher, J. Am. Chem. Soc. 23 (1985) 856.
[30] M.W. Schmidt, et al., J. Comput. Chem. 14 (1993) 1347.
[31] M.J. Frisch, et al., GAUSSIAN 03, Revision B.03, Gaussian, Inc., Pittsburgh, MA, 2003.
[32] W.J. Hehre, R. Ditchfield, J.A. Pople, J. Chem. Phys. 56 (1972) 2257.
[33] T.H. Dunning Jr., J. Chem. Phys. 44 (1971) 2356.
[34] A.D. McClean, G.S. Chandler, J. Chem. Phys. 44 (1971) 2356.
[35] A.J.H. Watchers, J. Chem. Phys. 44 (1971) 2356.
[36] G. Knuchel, G. Grassi, B. Vogelsanger, A. Bauder, Magn. Res. Chem. 115 (1993) 10845.
[37] J.F. Chiang, R. Chiang, K.C. Lu, E.M. Sung, M.D. Harmony, J. Mol. Struct. (Theochem) 165 (1987) 241.
[38] J. Benet-Buchholz, T. Haumann, R. Boese, J. Chem. Soc. Chem. Commun. 1998; 2003.
[39] F. Wang, M.J. Brunger, D.A. Winkler, M. Hamilton, B. Appelbe, Bioactive discovery in the new millennium, A Joint RACI, JMGM, FACS and MM Conference, Lorne, Vic., Australia, February 5–9, 2003.
[40] S. Inagaki, H. Fujimoto, K. Fukui, J. Am. Chem. Soc. 98 (1976) 4056.
[41] G. Wipff, K. Morokuma, Tetrahedron Lett. 21 (1980) 4445.
[42] T. van Auken, E.A. Rick, Tetrahedron Lett. 22 (1968) 2712.
[43] A. Yokozeki, A. Kuchitsu, Bull. Chem. Soc. Jpn 44 (1971) 2356.
[44] H.O. Ohorodnyk, D.P. Santry, J. Am. Chem. Soc. 91 (1969) 4711.
[45] A. Choplin, Chem. Phys. Lett. 71 (1980) 503.
[46] F. Wang, J. Phys. Chem. A 107 (2003) 10199.
[47] N. Godbout, D.R. Salahub, J. Anddzelm, E. Wimmer, Can. J. Chem. 70 (1992) 560.
[48] M.N. Paddon-Row, S. Wong, K.D. Jordan, J. Am. Chem. Soc. 112 (1990) 1710.
[49] K.B. Wiberg, G. Bonneville, R. Dempsey, Isr. J. Chem. 23 (1983) 85.